

Highlights

PreMix: Addressing Label Scarcity in Whole Slide Image Classification with Pre-trained Multiple Instance Learning Aggregators

Bryan Wong, Mun Yong Yi

- This study introduces PreMix, a framework that leverages the Barlow Twins method with a Slide Mixing approach to pre-train MIL aggregators, addressing the scarce labeled WSIs and the underexplored potential of utilizing unlabeled WSIs in weakly supervised classification.
- Fine-tuning with Mixup and Manifold Mixup further enhances robustness by effectively handling the diverse sizes of gigapixel WSIs.
- Experimental results demonstrate that integrating HIPT into PreMix achieves a 4.7% mean F1 improvement over the baseline HIPT, showcasing its scalability and effectiveness across varying WSI datasets and labeling scenarios.

PreMix: Addressing Label Scarcity in Whole Slide Image Classification with Pre-trained Multiple Instance Learning Aggregators

Bryan Wong^a, Mun Yong Yi^{a,b,*}

^aGraduate School of Data Science, KAIST, Daejeon, 34141, Republic of Korea

^bDepartment of Industrial and Systems Engineering, KAIST, Daejeon, 34141, Republic of Korea

ARTICLE INFO

Keywords:

Whole slide image
Weakly-supervised classification
Multiple instance learning
Self-supervised learning
Data scarcity
Data augmentation

Abstract

Multiple instance learning (MIL) has emerged as a powerful framework for weakly supervised whole slide image (WSI) classification, enabling slide-level predictions without requiring detailed patch-level annotations. However, a key limitation of MIL lies in the underexplored potential of pre-training the MIL aggregator. Most existing approaches train it from scratch, resulting in performance heavily dependent on the number of labeled WSIs, while overlooking the abundance of unlabeled WSIs available in real-world scenarios. To address this, we propose PreMix, a novel framework that leverages a non-contrastive pre-training method, Barlow Twins, augmented with the Slide Mixing approach to generate additional positive pairs and enhance feature learning, particularly under limited labeled WSI conditions. Fine-tuning with Mixup and Manifold Mixup further enhances robustness by effectively handling the diverse sizes of gigapixel WSIs. Experimental results demonstrate that integrating HIPT into PreMix achieves an average F1 improvement of 4.7% over the baseline HIPT across various WSI training datasets and label sizes. These findings underscore its potential to advance WSI classification with limited labeled data and its applicability to real-world histopathology practices. The code is available at <https://anonymous.4open.science/r/PreMix>

1. Introduction

Histopathology, the study of tissues under a microscope, is essential for diagnosing diseases, predicting outcomes, and planning treatments [1]. Traditionally, this process relied heavily on the expertise of trained professionals analyzing tissue samples. However, advancements in medical imaging have significantly transformed the field. One of the most notable developments is the use of whole slide images (WSIs), which digitally capture detailed views of tissue samples for digital pathology [2]. These high-resolution images offer deep insights into tissue structures and abnormalities, enabling more effective diagnosis and treatment planning [3, 4]. However, this advancement comes with complexities. The vast scale of WSIs, characterized by gigapixel resolution, and the often subtle disease indications pose challenges for both computer professionals and medical practitioners [5].


The immense size of WSIs makes it impractical to directly train deep-learning models on them without preprocessing into smaller patches, given current GPU limitations. Additionally, annotating WSIs is time-consuming and costly due to their resolution, and manual labeling is prone to errors and inconsistencies [6]. To address these challenges, multiple instance learning (MIL) offers a weakly-supervised approach for WSI classification, particularly useful for clinical pre-screening. MIL accommodates varying WSI sizes and relies only on slide-level labels, eliminating the need for labor-intensive patch-level annotations. By reducing dependency on detailed labels, MIL overcomes the limitations of

traditional supervised methods and provides a more robust and efficient solution for WSI analysis [7].

As shown in Figure 1(a), the MIL process typically involves tiling WSIs into patches, processing these patches through a pre-trained feature extractor (e.g., CNN or ViT), and generating either scalar outputs (instance-based MIL) or feature vectors (embedding-based MIL). Among these approaches, embedding-based MIL, which provides richer representations, has been shown to be more effective for WSI classification [8]. The outputs are then aggregated using an MIL aggregator for slide-level prediction. However, existing MIL approaches [9, 10, 11, 12, 13, 14, 15] typically train the MIL aggregator from scratch, which limits performance when only a small number of labeled WSIs are available.

We argue that improving WSI classification performance with a limited number of labeled training WSIs requires leveraging the abundance of unlabeled WSIs, reflecting the common real-world scenario where many WSIs remain unlabeled. By utilizing these unlabeled WSIs and employing a proper pre-training method for the MIL aggregator, we aim to achieve better initialization, leading to enhanced WSI classification performance. While we are not the first to explore MIL aggregator pre-training, SSMIL [16] pioneered the use of the SimCLR [17] contrastive method for pre-training MIL aggregators at the WSI level. However, this approach has been shown to underperform compared to training the MIL aggregator from scratch. We attribute this limitation to the inherent imbalance in gigapixel WSI datasets (e.g., a significantly larger number of normal WSIs compared to tumor WSIs), which often leads to the inclusion of incorrect or noisy negative pairs—a critical issue for contrastive methods reliant on both positive and negative pairs.

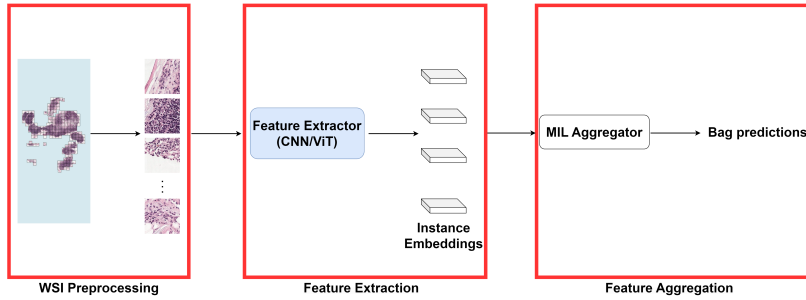
*Corresponding author: munyi@kaist.ac.kr

 bryan.wong@kaist.ac.kr (B. Wong); munyi@kaist.ac.kr (M.Y. Yi)

ORCID(s): 0000-0002-2257-3454 (B. Wong); 0000-0003-1784-8983

(M.Y. Yi)

(a) Common MIL Framework



(b) PreMix (Proposed) Framework

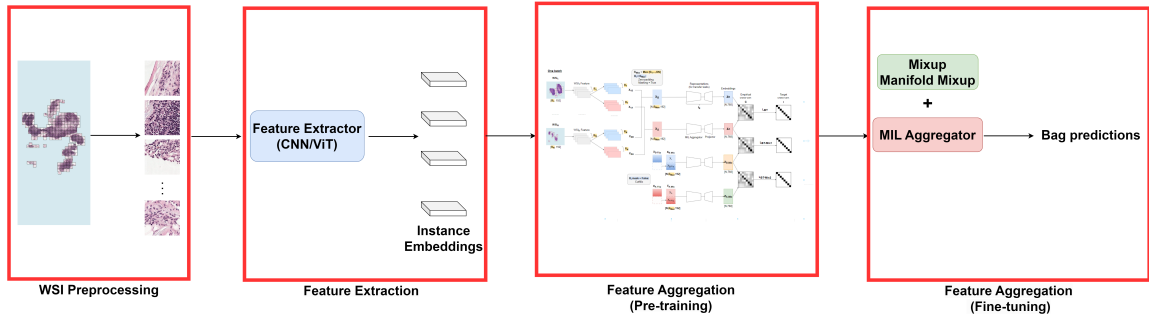


Figure 1: (a) In the common MIL framework, instance embeddings are extracted from the pre-trained feature extractor and the MIL aggregator is trained from scratch to get bag predictions. (b) In our proposed framework, PreMix, the MIL aggregator is pre-trained using unlabeled WSIs with Barlow Twins Slide Mixing (see Section 3.4.1) and further fine-tuned with Mixup and Manifold Mixup (see Section 3.4.2). For a fair comparison, we use the original HIPT as the baseline and evaluate the integration of HIPT into PreMix.

To address these challenges, we propose the PreMix (**Pre-training** and **Mixing**) framework (see Figure 1(b)). The core innovation of PreMix lies in adopting a non-contrastive approach, Barlow Twins [18], as the base pre-training method. Barlow Twins relies solely on positive pairs, eliminating the need for negative pairs. We extend this method with an intra-batch mixing strategy, termed Barlow Twins Slide Mixing, to generate additional positive pairs from unlabeled WSIs. This approach leverages the semantic relatedness of mixed slide features, even when they originate from different slides within the same batch, to enrich the pre-training process.

To further enhance robustness and generalization, we incorporate Mixup [19] and Manifold Mixup [20] during the fine-tuning stage. These techniques are adapted to handle the unique challenges of WSIs, enabling the mixing of features and labels across slides of varying sizes within the batch. The PreMix framework is evaluated using HIPT [21] as the baseline, and we demonstrate its effectiveness by integrating HIPT into PreMix to validate its generalizability across different training datasets and sample sizes.

The main contributions of this paper are as follows:

- We identify the limitations of contrastive learning methods (e.g., SimCLR) for MIL aggregator pre-training, as they hinder WSI classification performance. Instead, we propose the use of non-contrastive learning methods (e.g., Barlow Twins), which do not require negative pairs and are more suitable for imbalanced gigapixel WSI datasets, achieving better classification results.
- We introduce PreMix, an extension of the general MIL framework, which enhances the MIL aggregator by pre-training it with the novel Barlow Twins Slide Mixing approach. This method extends Barlow Twins by incorporating intra-batch mixing to generate additional positive pairs, improving feature representation during pre-training.
- We integrate Mixup and Manifold Mixup during MIL aggregator fine-tuning, enabling WSI feature and label mixing across different WSI feature sizes. Furthermore, we demonstrate that applying Manifold Mixup at the Transformer Encoder layer yields the most significant performance improvements.
- To validate the proposed MIL aggregator pre-training method under limited labeling scenarios, we conduct experiments with five different WSI training sample

sizes. Additionally, we evaluate its robustness across datasets using random sampling (traditional fully-supervised fine-tuning) and five active learning acquisition functions: Entropy, K-means++, Coreset, BADGE, and CDAL. These experiments demonstrate the framework's robustness across varying WSI datasets and training sizes, highlighting its versatility and effectiveness.

The remainder of this paper is organized as follows: Section 2 introduces related literature, including self-supervised learning for pre-training in the histopathology domain, MIL in histopathology domain at both single and multi scales, existing data augmentation strategies. Section 3 details the problem formulation, overall training process, and the proposed framework. Section 4 describes the dataset, implementation setup, model evaluation, experiment results, and ablation studies. In Section 5, we discuss our findings and future research directions. Finally, we conclude our paper in Section 6.

2. Related Work

2.1. Self-supervised learning in histopathology

In the medical field, where obtaining expert annotations is challenging and expensive, self-supervised learning (SSL) has emerged as a promising solution since it does not rely on labeled data [22]. Ciga et al. [23] demonstrated the effectiveness of the SimCLR method [17] for pre-training models in histopathology. Their work highlighted the robustness of patch-level feature representations for various downstream tasks. Building on this, Chen and Krishnan [24] proposed replacing SimCLR-trained ResNet-50 encoders [25] with ViTs [26], leveraging the DINO method [27] to better capture intricate details of histopathological tissues. Kang et al. [28] further conducted a comprehensive evaluation of SSL methods in histopathology, comparing four representative SSL approaches: Barlow Twins [18], SwAV [29], MoCo V2 [30], and DINO [27]. Recently, Wong and Yi [31] provided practical guidance on optimizing WSI classification by analyzing feature extractors from three dimensions: pre-training dataset, backbone model, and pre-training method.

While most SSL studies in histopathology focus on learning patch-level feature representations, SSMIL [16] stands out as the first to explore pre-training the MIL aggregator using SimCLR [17]. However, MIL aggregators fine-tuned using this approach still underperform compared to those trained from scratch, highlighting the need for more effective pre-training strategies.

2.2. Multiple instance learning for WSI analysis

Recent advancements in multiple instance learning (MIL) for WSI classification have moved beyond traditional aggregation methods, such as mean or max pooling, to techniques that extract and combine patch-level features for slide-level predictions [32]. Early methods like MIL-RNN [9] aggregates patch features across slides but struggled with long-distance information loss due to the large number of

patches. To address these spatial complexities, ABMIL [10] computes attention scores for each patch, while DSMIL [11] applies distances between instances and a critical instance as weights. CLAM [12] refines feature spaces through instance-level clustering, while TransMIL [33] uses a transformer architecture to capture relationships among patches. DTFD-MIL [34] addresses data limitations in WSIs by introducing pseudo-bags and calculating instance probabilities under the ABMIL framework. Recently, MHIM-MIL [35] focuses on identifying hard-to-classify instances using a momentum teacher to train attention-based MIL models.

Despite their effectiveness, single-scale methods are limited by their inability to capture spatial correlations across resolutions. Multi-resolution strategies address this limitation by leveraging features from multiple magnifications. DSMIL-LC [11] concatenates low- and high-resolution features to improve context-awareness. HIPT [21] employs a hierarchical transformer to extract detailed and contextual features across scales, while MS-DA-MIL [36], H²-MIL [37], and DAS-MIL [38] use graph-based models to enhance spatial and scaling relationships between patches.

HIPT's hierarchical feature extraction process stands out for its ability to efficiently combine detail and context across scales, making it particularly suitable for both pre-training and downstream classification tasks. Motivated by these advantages, we adopt the original HIPT as the baseline and evaluate its performance within the PreMix framework to demonstrate its effectiveness.

2.3. Data augmentation

To address the challenges of limited data and improve deep learning performance, various data augmentation techniques have been developed [39]. One prominent method is Mixup [19], which blends images and their labels to enhance classification, inspiring numerous domain-specific techniques such as Balanced Mixup [40] and Stain Mixup [41]. The integration of such data mixing methods into SSL has led to significant improvements. For example, Ren et al. [42] demonstrated that incorporating mixed natural images as supplementary positive pairs during pre-training enhanced the performance of MoCo V2.

While many augmentation techniques are designed for natural images or specific medical applications, the unique challenges of WSIs, such as their gigapixel size and diverse feature scales, have led to the development of specialized solutions. Methods like ReMix [32], RankMix [43], and PseMix [44] focus on downstream classification, adapting data augmentation techniques to the WSI domain. In contrast, our approach incorporates data augmentation during both pre-training and downstream classification. Specifically, we employ an intra-batch mixing approach during the pre-training of the MIL aggregator at the WSI level, enabling the generation of additional positive pairs while handling diverse WSI feature sizes. In downstream classification, we adapt Mixup [19] and Manifold Mixup [20] to combine WSI features and labels of different sizes. Originally developed for natural images of consistent size, these methods are

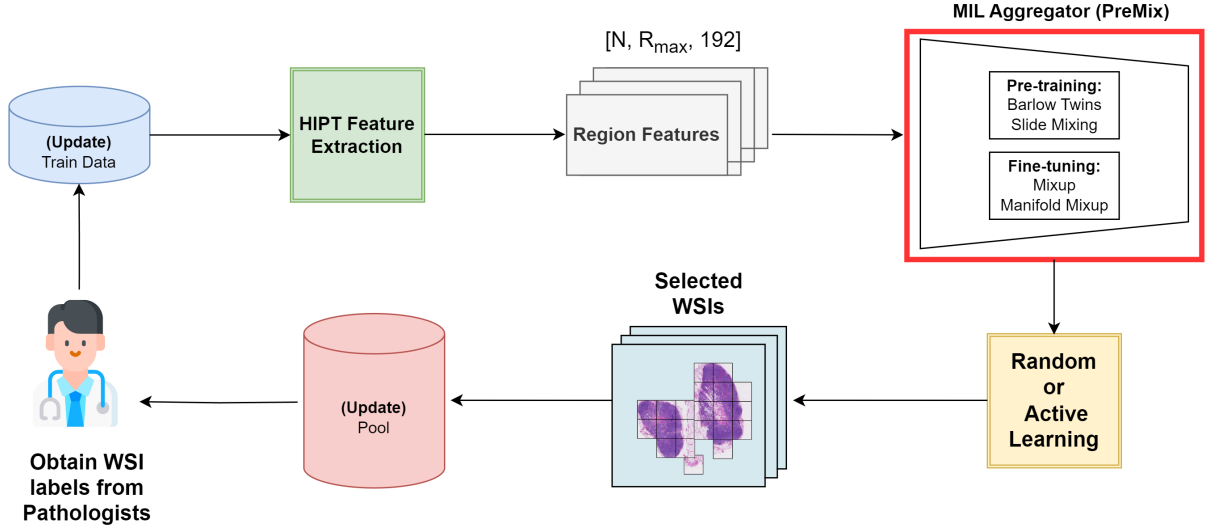


Figure 2: The illustration of our training process utilizing the HIPT feature extraction method showcases the selection of WSI candidates for labeling using either random sampling (traditional fully-supervised fine-tuning) or active learning. The selected WSIs are weakly-labeled by pathologists and incorporated into the next training iteration. A key distinction between the baseline HIPT and our HIPT with PreMix is that the latter incorporates MIL aggregator initialization from Barlow Twins Slide Mixing pre-training and employs Mixup and Manifold Mixup during fine-tuning, while the baseline does not.

modified to address the unique characteristics of WSIs, improving performance and robustness.

3. Methods

3.1. General MIL framework

As illustrated in Figure 1(a), a common MIL framework consists of two key steps after WSI preprocessing: feature extraction and feature aggregation.

3.1.1. Feature extraction

Given a WSI denoted by the index i , where raw patches, typically of size 224×224 pixels, are extracted, forming the set $X_i = \{x_{i,1}, x_{i,2}, x_{i,3}, \dots, x_{i,n(i)}\}$. Each of these patches undergoes processing through a pre-trained patch feature extractor denoted as f_p , commonly implemented using architectures like ResNet [25] or ViT [26]. This extraction procedure results in a set of feature representations, $P_i = \{p_{i,1}, p_{i,2}, p_{i,3}, \dots, p_{i,n(i)}\} \in \mathbb{R}^{n(i) \times d}$, where $n(i)$ represents the variable number of patches extracted from the WSI X_i , and d denotes the feature length determined by the chosen patch feature extractor.

3.1.2. Feature aggregation

After extraction, the individual patch features are aggregated to form a slide-level representation. This feature aggregation process is facilitated by the MIL aggregator, f_a . In most cases, f_a is trained from scratch. This process yields a comprehensive slide-level representation, expressed as $f_a(P_i) \in \mathbb{R}^{1 \times d}$. The primary objective of this step is to conduct the binary classification of slides. Consequently,

the final representations are fed into a linear classifier to distinguish between two classes. Each slide is assigned a label $Y_i \in \{0, 1\}$, where a slide is labeled as $Y_i = 0$ if it is normal and $Y_i = 1$ if it contains tumor.

3.2. HIPT feature extraction

Contrary to most MIL methods [11, 12, 15, 14], which predominantly focus on single-level feature extraction (see Section 3.1.1), our experiment employs hierarchical visual token representations from HIPT [21] across various image resolutions. This approach provides a more efficient feature set and captures spatial relationships that are beneficial for both pre-training and downstream classification phases.

In this process, each WSI undergoes tiling into multiple regions, each sized $[4096, 4096]$ pixels. Subsequently, the slides are resized to the format $[R, 256, 3, 256, 256]$ with R representing the number of regions in a given slide. These resized regions are then input into the pre-trained self-supervised ViT DINO 256 (1st stage) [27], resulting in slide dimensions of $[R, 256, 384]$. Here, 256 signifies the sequence length of $[CLS]$ tokens. The outputs are subsequently reshaped to $[R, 384, 16, 16]$ and fed into the pre-trained self-supervised ViT DINO 4k (2nd stage). This final process yields a single slide representation of $[R, 192]$.

3.3. Overall training process

In Figure 2, we present an overview of the comprehensive training process used in our experimental settings. Initially, we randomly select 20 WSIs, tile them into multiple regions each sized $[4096, 4096]$ pixels, and process them

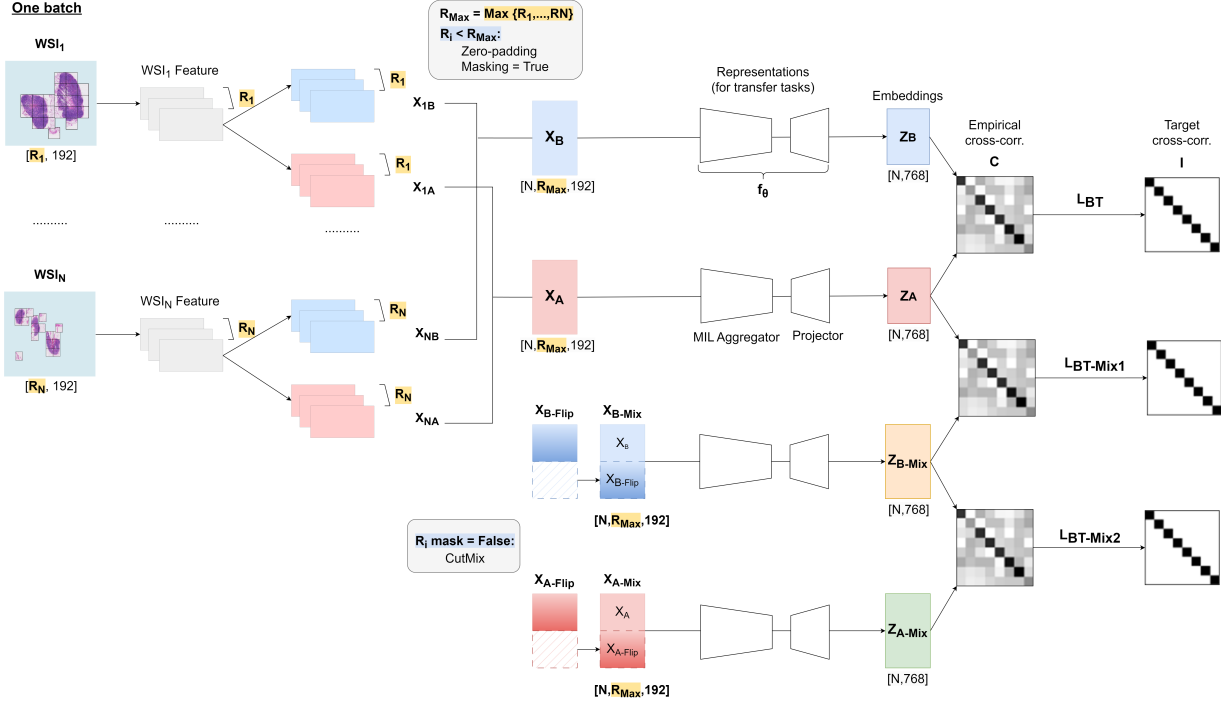


Figure 3: Barlow Twins Slide Mixing: This process relies on region features extracted via HIPT as inputs, accommodating varying WSI input sizes through zero-padding and masking techniques and the addition of intra-batch mixing strategy during pre-training. "Flip" means from the same batch but with the batch order reversed.

using the HIPT feature extraction method (see Section 3.2). The resulting dimensions are $[N, R_{max}, 192]$, where N is the batch size, R_{max} represents the maximum number of regions per WSI in a batch, and 192 denotes the dimensionality of the ViT DINO CLS tokens at the region level.

For the baseline, we initialize the MIL aggregator from scratch. Meanwhile, for our proposed framework, we first pre-train the MIL aggregator using the Barlow Twins Slide Mixing method (see Section 3.4.1) and then incorporate Mixup and Manifold Mixup during the fine-tuning process (see Section 3.4.2). After processing through the MIL aggregator and linear classifier, the output shape for both the baseline and proposed frameworks is $[N, num_classes]$, representing the predicted probability for each class.

Finally, the most informative WSIs, determined by active learning acquisition functions or random sampling are selected from the unlabeled pool. These selected WSIs are then labeled by pathologists in a weakly-supervised setting, requiring only slide-level labels without fine-grained annotations. Subsequently, they are added to the training data for the next cycle. This process continues until the total labeling budget for WSIs (number of available WSIs and their labels) is exhausted.

3.4. PreMix

The distinction between the original MIL framework and the PreMix lies in the pre-training MIL aggregator using Barlow Twins Slide Mixing (see Section 3.4.1) and the use of

Mixup and Manifold Mixup during fine-tuning (see Section 3.4.2), whereas the original MIL framework trains the MIL aggregator directly from scratch.

3.4.1. Pre-training: Barlow Twins Slide Mixing

Initializing neural networks with pre-trained models offers the advantage of leveraging knowledge from unlabeled datasets, providing a strong starting point with weights that capture general patterns and representations. This strategy is particularly beneficial for tasks with limited labeled data [45].

The core focus of PreMix is to improve the MIL aggregator through better initialization, ultimately enhancing downstream WSI classification performance. This approach maximizes the use of unlabeled WSIs, making it especially valuable in scenarios with limited labeled data. To achieve this, we adopt the Barlow Twins method [18] as the base non-contrastive SSL method and introduce an intra-batch mixing strategy to generate additional positive pairs. Since WSIs can produce varying numbers of region features, we apply zero-padding and masking techniques to ensure consistent batch dimensions during pre-training.

Slide augmentation. Standard augmentations from the *PyTorch torchvision* library [46] are not directly applicable in our context, as our inputs are extracted WSI features rather than natural images. To address this limitation, we adapt four specific augmentations—random zeroing, Gaussian noise addition, random scaling, and random cropping—so they

can be applied to WSI features during pre-training. As shown in Figure 3, for the N^{th} WSI in the batch, the augmented features are denoted as X_{NA} and X_{NB} . After applying augmentations to all WSIs in the batch, the features X_{1A} to X_{NA} are combined into X_A , and similarly, X_{1B} to X_{NB} are combined into X_B .

Intra-batch mixing. Inspired by prior work [42], which demonstrated the effectiveness of image mixing in MoCo V2 [30] for improving downstream image classification, we introduce an intra-batch mixing strategy to the Barlow Twins method (a non-contrastive approach) to enhance the generation of positive slide pairs during MIL aggregator pre-training. Specifically, slide mixing is performed within a single batch to produce additional inputs, denoted as $X_{A-\text{Mix}}$ and $X_{B-\text{Mix}}$, as illustrated in Figure 3.

Within the batch of WSI features, each feature indexed by i is assigned a mixing coefficient $\lambda(i)$, sampled from a Beta distribution to determine the mixing proportion. To ensure balanced mixing, $\lambda(i)$ is transformed to fall within the interval $[0.1, 0.9]$, resulting in a balanced mixing proportion. The modified mixing proportion, denoted as $ratio(i)$, is then defined as:

$$ratio(i) = \sqrt{1 - (0.8 \times \lambda(i) + 0.1)} \quad (1)$$

To identify the number of non-padding regions in the slides, we calculate:

$$non_pad_len(i) = \sum_i \neg mask(i) \quad (2)$$

The number of regions selected for mixing, relative to the total number of non-padding regions, is determined as:

$$cut_len(i) = ratio(i) \times non_pad_len(i) \quad (3)$$

To define the boundaries of the selected regions, a random center point $cr(i)$ is chosen, and it is computed as:

$$cr(i) = Rand \left(\frac{cut_len(i)}{2}, non_pad_len(i) - \frac{cut_len(i)}{2} \right) \quad (4)$$

From the center point, the start and end indices of the regions are inferred as:

$$\begin{aligned} start_idx(i) &= cr(i) - \frac{cut_len(i)}{2}, \\ end_idx(i) &= cr(i) + \frac{cut_len(i)}{2} \end{aligned} \quad (5)$$

It is crucial to ensure that the selected regions for mixing do not intersect with the masked regions. This condition is enforced by:

$$mask[start_idx(i) : end_idx(i)] = \emptyset \quad (6)$$

To generate the new slide-mixed feature ($X_{A-\text{Mix}}$), a feature $X_A(i)$ is mixed with another feature $X_{A-\text{Flip}}(i)$, where

$X_{A-\text{Flip}}(i)$ is obtained by reversing the batch order. This process increases the generation of positive slide pairs, providing additional inputs for pre-training compared to the original Barlow Twins method. The resulting slide-mixed feature enhances the diversity of training data and improves feature representation during pre-training.

$$\begin{aligned} X_A[i, start_idx(i) : end_idx(i), :] \\ = X_{A-\text{Flip}}[i, start_idx(i) : end_idx(i), :] \end{aligned} \quad (7)$$

Pre-training loss. From Equation 7, we derive $X_{A-\text{Mix}}$ by mixing X_A and $X_{A-\text{Flip}}$, and similarly, $X_{B-\text{Mix}}$ is obtained by mixing X_B and $X_{B-\text{Flip}}$. These inputs, X_A , X_B , $X_{A-\text{Mix}}$, and $X_{B-\text{Mix}}$, are then passed through an MIL aggregator and a projector to produce the corresponding slide embeddings Z_A , Z_B , $Z_{A-\text{Mix}}$, and $Z_{B-\text{Mix}}$.

To incorporate the mixing proportion during intra-batch mixing for loss calculation, we define $\lambda(i)$ as:

$$lam(i) = 1 - \frac{cut_len(i)}{non_pad_len(i)} \quad (8)$$

The details of the ORIGINALLOSS and MIXINGLOSS functions, used to compute the Barlow Twins Slide Mixing loss, are provided in Algorithm 1. The ORIGINALLOSS function calculates the standard Barlow Twins loss, while the MIXINGLOSS function computes the loss between $Z_{B-\text{Mix}}$ and Z_A or $Z_{B-\text{Mix}}$ and $Z_{A-\text{Mix}}$, accounting for $\lambda(i)$ as defined above. Here, "Flip" refers to reversing the batch order.

The total loss has three main components: *source_loss*, which is the loss between Z_A and Z_B calculated using the ORIGINALLOSS function; *mix_source_loss*, which is the loss between $Z_{B-\text{Mix}}$ and Z_A ; and *mix_loss*, which represents the loss between $Z_{B-\text{Mix}}$ and $Z_{A-\text{Mix}}$, both computed using the MIXINGLOSS function.

$$\begin{aligned} source_loss &\leftarrow ORIGINALLOSS(Z_A, Z_B) \\ mix_source_loss &\leftarrow MIXLOSS(Z_{B-\text{Mix}}, Z_A, \lambda, 1 - \lambda) \\ com &\leftarrow \min(\lambda, 1 - flip(\lambda)) + \min(1 - \lambda, flip(\lambda)) \\ mix_loss &\leftarrow MIXLOSS(Z_{B-\text{Mix}}, Z_{A-\text{Mix}}, \frac{1}{1 + com}, \frac{com}{1 + com}) \end{aligned} \quad (9)$$

The total loss is defined as follows:

$$total_loss = \alpha \cdot source_loss + \beta \cdot mix_source_loss + \gamma \cdot mix_loss \quad (10)$$

Where α , β , and γ are hyperparameters of the model that control the weight of each loss component in the total loss.

3.4.2. Fine-tuning: Mixup and Manifold Mixup

Data augmentation techniques like Mixup [19] and Manifold Mixup [20] are widely used to enhance model performance by generating additional training samples. These

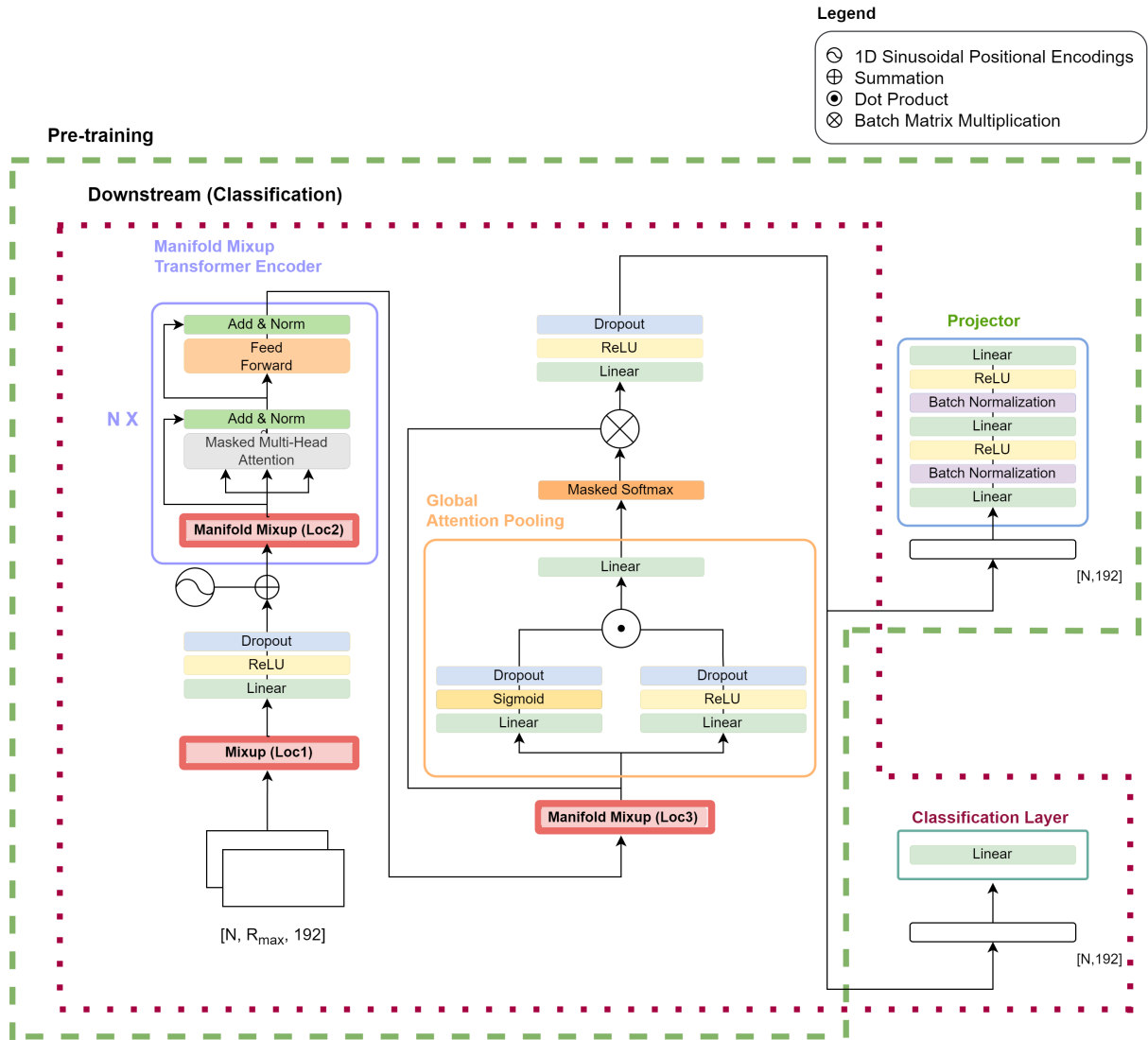


Figure 4: The MIL aggregator architecture supports two tasks: (1) Pre-training and (2) Downstream Classification. For pre-training, it includes components such as the Manifold Mixup Transformer Encoder, Global Attention Pooling, and Projector. For classification, it utilizes the Manifold Mixup Transformer Encoder, Global Attention Pooling, and a Classification Layer. This architecture extends the original HIPT design by incorporating positional encodings, leveraging enhanced initialization from pre-training, and employing slide feature mixing during fine-tuning (highlighted in red).

methods create interpolations between data points and their labels, introducing greater variability and robustness into the training process. The primary distinction between Mixup and Manifold Mixup lies in their application: Mixup operates directly on input features, while Manifold Mixup is applied within the hidden layers of a neural network, enabling interpolations in the feature space.

In our work, we extend both Mixup and Manifold Mixup to handle the unique challenges of WSIs, where feature and label mixing involves data from varying WSI feature sizes within a single training batch. Unlike the original implementations [19, 20], which were designed for natural images with uniform dimensions, our approach accommodates the

size variability common in WSIs. This adaptation makes the proposed method particularly effective for this domain, where feature dimensions can differ significantly between samples.

To manage the varying feature dimensions of WSIs, we standardize their shapes using zero padding and apply masking to exclude padded regions from computations. We also modify key components of the MIL aggregator, implementing masked multi-head self-attention and masked softmax operations to focus computations exclusively on non-padded regions. The detailed architecture of the MIL aggregator, including the integration points for Mixup and Manifold Mixup, is shown in Figure 4.

Table 1

WSI dataset distribution during pre-training and downstream classification phases. An "x" indicates that the dataset is not used in a particular process (e.g., pre-training, training, or testing), while a "-" indicates that distributions depend on the random sampling or active learning (AL) strategy used to select a 20 WSI sample budget per iteration from the unlabeled pool.

Phase	Dataset	Iteration	Pre-training		Train		Test	
			Normal	Tumor	Normal	Tumor	Normal	Tumor
Pre-training	Camelyon16 CPTAC UCEC	x	159	111	x	x	x	x
			185	390				
Classification	Camelyon16	1st (Random)	x	x	12	8	80	49
		2nd - 5th (Rand or AL, Budget: 20)			-	-		

Algorithm 1 Barlow Twins Slide Mixing Loss Calculation

Input: Slide embeddings: Z_A, Z_B ; Mixed slide embeddings:

Z_{A-Mix}, Z_{B-Mix} ; Mixing coefficient: lam

Output: Loss values: $source_loss, mix_source_loss, mix_loss$

```

1: function ORIGINALLOSS( $Z_A, Z_B$ )
2:    $C \leftarrow \frac{1}{batch\_size} \cdot BatchNorm1d(Z_A)^T \cdot BatchNorm1d(Z_B)$ 
3:    $on\_diag \leftarrow \sum(diag(C) - 1)^2$ 
4:    $off\_diag \leftarrow \sum off\_diagonal(C)^2$ 
5:    $loss \leftarrow on\_diag + \lambda_{BT} \cdot off\_diag$ 
6:   return  $loss$ 
7: end function
8: function MIXLOSS( $Z_A, Z_B, lam_A, lam_B$ )
9:    $original\_loss \leftarrow ORIGINALLOSS(Z_A, Z_B)$ 
10:   $flip\_loss \leftarrow ORIGINALLOSS(Z_A, flip(Z_B))$ 
11:   $mix\_loss \leftarrow lam_A \cdot original\_loss + lam_B \cdot flip\_loss$ 
12:  return  $mean(mix\_loss)$ 
13: end function

```

Mixup is applied at the input stage (*Loc1*), where input features are randomly interpolated. Manifold Mixup is applied consistently within the Transformer Encoder layer (*Loc2*) and at its output (*Loc3*) to create interpolations in the feature space. These augmentations are designed to improve model robustness and generalization during fine-tuning.

4. Experiments

4.1. Data acquisition and preparation

This study utilizes the Camelyon16 dataset [47]¹, which contains 399 hematoxylin and eosin (H&E) stained whole slide images (WSIs) of breast cancer lymph node sections collected from two hospitals in the Netherlands: Radboud University Medical Center (RUMC) and University Medical Center Utrecht (UMCU). The dataset is divided into 270 training slides (159 normal and 111 tumor) and 129 test slides, serving as a widely used benchmark for WSI classification tasks.

For the pre-training phase, we supplement Camelyon16 with data from the Clinical Proteomic Tumor Analysis Consortium (CPTAC) Uterine Corpus Endometrial Carcinoma (UCEC) dataset [48]². From this dataset, 575 H&E stained WSIs of endometrial tissue samples are selected, comprising 185 normal and 390 tumor slides. The UCEC dataset

¹Link to Camelyon16 dataset

²Link to CPTAC UCEC dataset

focuses on endometrial cancer, a significant gynecological malignancy, providing diverse tissue samples for robust representation learning. During pre-training, both Camelyon16 and UCEC datasets are utilized in an unsupervised manner, with no access to slide-level labels to ensure a purely self-supervised learning process. All test data are strictly excluded from the pre-training phase to prevent information leakage.

To evaluate the model's performance in data-limited scenarios, we restrict training to 100 WSIs from the Camelyon16 dataset. Initially, 20 WSIs are randomly selected for training, followed by iterative sample selection using either random sampling or active learning acquisition functions [49, 50, 51, 52, 53]. The complete Camelyon16 test set of 129 WSIs is retained for final evaluation. A detailed summary of the WSI dataset distribution across the pre-training and downstream classification phases is provided in Table 1.

4.2. Implementation setup

To operate under resource constraints and demonstrate the efficiency of our framework, all training experiments, including pre-training and downstream classification, are conducted on a single NVIDIA GeForce RTX 2080 Ti GPU. The models are implemented and trained using the *PyTorch* library [46], a widely used open-source deep learning platform, with all experiments performed in Python. For tiling WSIs into distinct regions, we use the *OpenSlide* library [54].

4.2.1. Region extraction

WSIs are tiled into regions of size [4096, 4096] pixels with no overlap between adjacent regions. A tissue threshold of 0.1 is applied to exclude non-informative regions. To standardize tissue patch extraction and address magnification differences across scanners in the Camelyon16 dataset, we employ HS2P [55], based on CLAM [12], with a pixel-spacing set to 0.5 $\mu\text{m}/\text{px}$ (equivalent to 20x magnification).

4.2.2. Pre-training

Pre-training is conducted using the LARS optimizer [56] with a batch size of 32 over 700 epochs. The hyperparameters are adopted from the original Barlow Twins framework [18], including a lambda value of $\lambda_{BT} = 0.0051$, a base learning rate of 0.2, and 0.0048 for biases and batch normalization parameters. The learning rate is scaled by

Table 2

Comparison of the baseline and MIL aggregator initialization using various pre-training methods, evaluated with the F1 score.

# Train WSIs	20	40	60	80	100	Mean
HIPT (Baseline)						
Random	65.1	65.9	66.7	65.9	74.4	67.6
Entropy	65.1	68.2	76.7	72.9	72.9	71.2
BADGE	65.1	64.3	67.4	70.5	72.1	67.9
Coreset	65.1	64.3	71.3	79.1	79.8	71.9
K-Means++	65.1	64.3	72.1	74.4	71.3	69.5
CDAL	65.1	70.5	70.5	74.4	76.7	71.5
Mean	65.1	66.3	70.8	72.9	74.5	69.9
+ SimCLR						
Random	62.8	62.8	64.3	62.8	68.2	64.2
Entropy	62.8	67.4	67.4	64.3	74.4	67.3
BADGE	62.8	55.8	67.4	70.5	69.0	65.1
Coreset	62.8	67.4	66.7	65.9	65.1	65.6
K-Means++	62.8	55.8	69.0	65.9	75.2	65.7
CDAL	62.8	63.6	69.0	70.5	76.7	68.5
Mean	62.8	62.1	67.3	66.7	71.4	66.1
# Train WSIs	20	40	60	80	100	Mean
+ Barlow Twins						
Random	67.4	65.1	67.4	65.1	69.0	66.8
Entropy	67.4	72.1	79.8	79.8	79.8	75.8
BADGE	67.4	64.3	69.8	76.0	77.5	71.0
Coreset	67.4	71.3	73.6	75.2	75.2	72.6
K-Means++	67.4	62.0	71.3	73.6	79.1	70.7
CDAL	67.4	60.5	71.3	76.7	78.3	70.9
Mean	67.4	65.9	72.2	74.4	76.5	71.3
+ Barlow Twins Slide Mixing						
Random	69.8	68.2	73.6	70.5	72.9	71.0
Entropy	69.8	71.3	74.4	77.5	78.3	74.3
BADGE	69.8	65.9	73.6	78.3	78.3	73.2
Coreset	69.8	68.2	77.5	76.0	79.1	74.1
K-Means++	69.8	72.9	74.4	74.4	77.5	73.8
CDAL	69.8	67.4	71.3	76.7	80.6	73.2
Mean	69.8	69.0	74.2	75.6	77.8	73.3

the batch size and normalized to 256, with a 10-epoch warm-up period followed by a cosine decay schedule that reduced the learning rate by a factor of 1000. A weight decay parameter of 10^{-6} is applied consistently throughout the training process.

To improve robustness during pre-training, we apply modified augmentations designed for WSI input features. These included random horizontal flipping, random zeroing, Gaussian noise addition, random scaling, and random cropping. Each augmentation is applied with a probability of 50%, except for Gaussian noise, which is applied with a probability of 10%. For intra-batch mixing, coefficients λ are sampled from a Beta(1, 1) distribution, ensuring variation among samples within each batch. The loss function's hyperparameters α , β , and γ are set to 1, 0.5, and 0.5, respectively.

4.2.3. Downstream classification

Downstream classification experiments are conducted over 50 epochs with a batch size of 4. The cross-entropy loss is optimized using the Adam optimizer [57], with a learning rate of 2×10^{-4} and a weight decay of 10^{-5} . A StepLR scheduler is employed, with a step size of 50 epochs and a decay factor of 0.5. The training process starts with an initial subset of 20 WSIs and adds 20 more in each of the subsequent five iterations. For experiments involving Mixup and Manifold Mixup, mixing coefficients λ were sampled from a Beta(1, 1) distribution and applied uniformly across all samples within each batch to ensure consistency.

4.3. Model evaluation

Model evaluation is conducted on the entire Camelyon16 test set, comprising 129 WSIs. The experiments utilize random sampling and five active learning acquisition functions: Entropy [49], K-Means++ [50], Coreset [51], BADGE [52], and CDAL [53]. Performance is assessed across five WSI training label budgets: 20, 40, 60, 80, and 100 WSIs.

In the baseline framework, the MIL aggregator is initialized and trained from scratch. To evaluate the effectiveness of the proposed framework, we compute the average F1 for each active learning acquisition function and random sampling (traditional fully-supervised fine-tuning) across label budgets. This comprehensive evaluation highlights the robustness and adaptability of our framework under varying dataset compositions and labeling budgets.

4.4. Impact of MIL aggregator pre-training methods

Building on the findings of [16], which employs the contrastive SimCLR method for MIL aggregator pre-training, we evaluate the non-contrastive Barlow Twins method alongside our proposed Barlow Twins Slide Mixing approach. The results, summarized in Table 2, reveal a clear difference in performance between these methods. Pre-training the MIL aggregator with SimCLR results in a 3.8% reduction in mean F1 compared to the baseline (training the aggregator from scratch), averaged across random sampling (traditional fully-supervised fine-tuning) and five active learning acquisition functions. In contrast, the Barlow Twins method achieves a 1.4% improvement over the baseline, highlighting the advantages of non-contrastive approaches for this task.

Our proposed Barlow Twins Slide Mixing method enhances the vanilla Barlow Twins approach by introducing intra-batch mixing, which generates additional positive WSI pairs during pre-training. This improvement results in a further 2% increase in mean F1 compared to the vanilla Barlow Twins method. These results underscore the effectiveness of our pre-training strategy in improving WSI classification by leveraging better initialization methods using unlabeled WSIs.

Table 3

Overall Results: Average performance of various acquisition functions under different budget constraints, evaluated with the F1 score. 'SM' means Slide Mixing.

Methods	# WSI Training Labels					Mean
	20	40	60	80	100	
HIPT (Baseline)	65.1	66.3	70.8	72.9	74.5	69.9
+ Barlow Twins SM	69.8	69.0	74.2	75.6	<u>77.8</u>	73.3
+ Barlow Twins SM + Mixup	<u>68.2</u>	69.5	74.7	76.0	<u>77.8</u>	<u>73.2</u>
+ Barlow Twins SM + Mixup Manifold Mixup (PreMix)	69.8	72.2	<u>74.5</u>	78.2	78.4	74.6
Best Improvement Δ	+ 4.7	+ 5.9	+ 3.9	+ 5.3	+ 3.9	+ 4.7

Table 4

Effect of adjusting hyperparameters (α, β, γ) in Barlow Twins Slide Mixing loss, corresponding to $source_{loss}$, $mix_{source_{loss}}$, and mix_{loss} in Equation 10, respectively, evaluated with the F1 score.

+ Barlow Twins Slide Mixing			# WSI Training Labels					Mean
α	β	γ	20	40	60	80	100	
0	0.5	0.5	65.9	66.5	73.3	76.4	77.3	71.9
0	1	1	67.4	69.9	73.5	74.9	76.6	72.5
1	0.5	0.5	66.7	70.2	72.9	76.7	77.6	72.8
1	1	1	70.5	68.0	74.0	73.8	76.4	72.5

4.5. Impact of Mixup and Manifold Mixup integration

Table 3 reports the average performance across random sampling (traditional fully-supervised fine-tuning) and five active learning acquisition functions under five different WSI training label budgets. Integrating Mixup and Manifold Mixup during the MIL aggregator fine-tuning phase, following Barlow Twins Slide Mixing initialization, achieves the highest performance. Specifically, this approach delivers a substantial improvement of 1.3% compared to the configuration without Mixup and Manifold Mixup and a total improvement of 4.7% over the baseline. The performance gains are consistent across different acquisition strategies and budget constraints, demonstrating the robustness of our framework, particularly in scenarios with limited labeled WSIs. These findings emphasize the critical role of proper initialization through pre-training and the significant benefits of incorporating Mixup and Manifold Mixup during fine-tuning, ultimately contributing to enhanced WSI classification.

4.6. Ablation study

4.6.1. Effect of slide mixing loss hyperparameters

We investigate the impact of adjusting the hyperparameters (α, β, γ) in the Barlow Twins Slide Mixing method over 300 epochs. These hyperparameters control the relative weights of $source_{loss}$, $mix_{source_{loss}}$, and mix_{loss} in Equation 10. As summarized in Table 4, the optimal performance is achieved with hyperparameter values set to (1, 0.5, 0.5). Other configurations yield slightly lower mean F1, suggesting that the performance of Barlow Twins Slide Mixing is robust to moderate variations in loss hyperparameters. These results highlight the method's flexibility and effectiveness across a range of parameter settings.

4.6.2. Effect of Mixup and Manifold Mixup locations

We analyze the impact of applying Mixup and Manifold Mixup at different locations during MIL aggregator fine-tuning. This evaluation focuses on the performance of mixing at $Loc1$, $Loc2$, and $Loc3$, as illustrated in Figure 4. According to Table 5, incorporating mixing at all three locations achieves the highest mean F1 of 74.6%, outperforming other configurations. In contrast, applying mixing only at $Loc1$ results in a slight performance decline, underscoring the importance of leveraging multiple mixing locations. Notably, placing Manifold Mixup at $Loc2$, within the Transformer Encoder layer, proves particularly advantageous, yielding a mean F1 improvement of 2.5%. These findings highlight the synergistic benefits of comprehensive mixing across layers, with the Transformer Encoder layer playing a pivotal role in driving the greatest performance gains.

5. Discussion

Most existing works train the MIL aggregator from scratch, overlooking the valuable information present in unlabeled WSIs. Our findings indicate that fine-tuning the MIL aggregator with a contrastive method, such as SimCLR, performs worse than supervised training in improving WSI classification. This trend is consistent with prior work [16]. The primary limitation of contrastive methods lies in their reliance on negative pairs alongside positive pairs. This approach is unsuitable for pre-training the MIL aggregator at the WSI level because the inherent imbalance in gigapixel WSI datasets (e.g., a significantly larger number of normal WSIs compared to tumor WSIs) often results in the inclusion of incorrect or noisy negative pairs. To address this issue, we recommend adopting non-contrastive methods such as Barlow Twins, which rely solely on positive pairs. Our experimental results demonstrate that, unlike contrastive

Table 5

Effect of Mixup and Manifold Mixup at different combination locations when fine-tuning the MIL aggregator, evaluated with the F1 score. Refer to Figure 4 for details on *Loc1*, *Loc2*, and *Loc3*.

+ Barlow Twins Slide Mixing			# WSI Training Labels					Mean
<i>Loc1</i>	<i>Loc2</i>	<i>Loc3</i>	20	40	60	80	100	
✓	✗	✗	68.2	69.5	74.7	76.0	77.8	73.2
✓	✗	✓	65.9	70.7	73.4	74.3	76.1	72.1
✓	✓	✓	69.8	72.2	74.5	78.2	78.4	74.6

methods that perform worse than the baseline (training the MIL aggregator from scratch), the non-contrastive approach significantly enhances WSI classification performance.

The proposed Barlow Twins Slide Mixing method further builds on the vanilla Barlow Twins approach by introducing an intra-batch mixing strategy that generates additional positive slide pairs during pre-training. This strategy enriches the pre-training process by leveraging the semantic relatedness of mixed slide features, even when the mixed features originate from different slides within the same batch. This additional semantic diversity enables the MIL aggregator to learn more robust and meaningful representations.

To improve downstream performance, we integrate Mixup and Manifold Mixup, designed to handle the unique gigapixel nature and variable sizes of WSIs. Unlike their original implementations for natural images of uniform size, our adaptations interpolate features and labels across diverse WSI dimensions. These techniques serve as effective augmentation methods, generating synthetic WSIs that enhance the model’s ability to generalize to unseen data. Additionally, these mixing approaches help mitigate class imbalance by creating interpolated WSIs that better balance the representation of different classes.

Our ablation study demonstrates the robustness of our method to variations in slide mixing loss hyperparameters, showing that performance remains stable across different hyperparameter settings. This alleviates the need for extensive hyperparameter tuning, making the method practical and user-friendly. The choice of mixing locations within the MIL aggregator also plays a critical role in the effectiveness of these techniques. Specifically, incorporating Manifold Mixup within the Transformer Encoder layer provides the most significant performance improvement. This enhancement can be attributed to the richer and more abstract feature representations at this layer, where interpolations act as effective feature space regularization. By maintaining the contextual integrity of original WSIs, Manifold Mixup within the Transformer architecture ensures coherent learning and improved classification performance.

We validate the proposed framework across various WSI training dataset sizes and labeling conditions. Under traditional fully-supervised fine-tuning with random sampling, our framework consistently outperforms the baseline. In addition, in an active learning setting, we evaluate its effectiveness using five acquisition functions: Entropy, K-means++, Coreset, BADGE, and CDAL. These functions are used to select the most informative WSIs for training which results

in different dataset for training. Our results highlight that the proposed framework remains robust across varying WSI datasets and training sizes, demonstrating its versatility and effectiveness.

Limitations and Future Work. While our framework demonstrates significant performance improvements, the pre-training dataset is limited in terms of organ diversity and the number of WSIs. Expanding the dataset to include a broader range of organs and larger WSI collections would likely enhance the robustness and generalizability of the proposed methods. Despite these constraints, this study emphasizes the potential of the Barlow Twins Slide Mixing approach, showcasing the effectiveness of non-contrastive methods combined with intra-batch mixing for pre-training the MIL aggregator. By leveraging unlabeled WSIs, our framework provides a scalable solution for improving WSI classification, offering valuable insights for future research in weakly-supervised learning and histopathology.

6. Conclusions

MIL aggregator pre-training is a crucial yet underexplored area in weakly supervised WSI classification. Most existing approaches train MIL aggregators from scratch, overlooking the potential of unlabeled WSIs. This paper introduces PreMix, a framework designed to leverage extensive, underutilized unlabeled WSI datasets by employing Barlow Twins Slide Mixing for MIL aggregator pre-training. By incorporating Mixup and Manifold Mixup during fine-tuning, PreMix demonstrates robust performance across diverse WSI training datasets and labels, including traditional fully-supervised fine-tuning settings and five active learning techniques. The results highlight PreMix’s potential to enhance WSI classification with limited labeled data and its applicability to real-world histopathology practices.

CRedit authorship contribution statement

Bryan Wong: Conceptualization, Methodology, Software, Validation, Formal analysis, Investigation, Writing - original draft, Writing - review & editing, Visualization.
Mun Yong Yi: Resources, Visualization, Writing - review & editing, Supervision, Funding acquisition.

Declaration of competing interest

The authors declare that they have no known competing financial interests or personal relationships that could have appeared to influence the work reported in this paper.

Acknowledgements

This research was supported by the Seegene Medical Foundation, South Korea, under the project “Development of a Multimodal Artificial Intelligence-Based Computer-Aided Diagnosis System for Gastrointestinal Endoscopic Biopsies” (Grant Number: G01240151).

Code availability

The code is publicly available at <https://anonymous.4open.science/r/PreMix>

Data availability

The pathological image datasets utilized in this study are publicly accessible through the following repositories: Camelyon16 dataset and CPTAC UCEC dataset.

References

- [1] A. Madabhushi, G. Lee, Image analysis and machine learning in digital pathology: Challenges and opportunities, *Medical image analysis* 33 (2016) 170–175.
- [2] L. Pantanowitz, A. Sharma, A. B. Carter, T. Kurc, A. Sussman, J. Saltz, Twenty years of digital pathology: an overview of the road travelled, what is on the horizon, and the emergence of vendor-neutral archives, *Journal of pathology informatics* 9 (2018) 40.
- [3] L. Pantanowitz, P. N. Valenstein, A. J. Evans, K. J. Kaplan, J. D. Pfeifer, D. C. Wilbur, L. C. Collins, T. J. Colgan, Review of the current state of whole slide imaging in pathology, *Journal of pathology informatics* 2 (2011) 36.
- [4] A. Serag, A. Ion-Margineanu, H. Qureshi, R. McMillan, M.-J. Saint Martin, J. Diamond, P. O’Reilly, P. Hamilton, Translational ai and deep learning in diagnostic pathology, *Frontiers in medicine* 6 (2019) 185.
- [5] N. Dimitriou, O. Arandjelović, P. D. Caie, Deep learning for whole slide image analysis: an overview, *Frontiers in medicine* 6 (2019) 264.
- [6] C. Kang, C. Lee, H. Song, M. Ma, S. Pereira, Variability matters: Evaluating inter-rater variability in histopathology for robust cell detection, in: *European Conference on Computer Vision*, Springer, 2022, pp. 552–565.
- [7] O. Maron, T. Lozano-Pérez, A framework for multiple-instance learning, *Advances in neural information processing systems* 10 (1997).
- [8] J. Butke, T. Frick, F. Roghmann, S. F. El-Mashtoly, K. Gerwert, A. Mosig, End-to-end multiple instance learning for whole-slide cytopathology of urothelial carcinoma, in: *MICCAI Workshop on Computational Pathology*, PMLR, 2021, pp. 57–68.
- [9] G. Campanella, M. G. Hanna, L. Geneslaw, A. Miraflor, V. Werneck Krauss Silva, K. J. Busam, E. Brogi, V. E. Reuter, D. S. Klimstra, T. J. Fuchs, Clinical-grade computational pathology using weakly supervised deep learning on whole slide images, *Nature medicine* 25 (2019) 1301–1309.
- [10] M. Ilse, J. Tomczak, M. Welling, Attention-based deep multiple instance learning, in: *International conference on machine learning*, PMLR, 2018, pp. 2127–2136.
- [11] B. Li, Y. Li, K. W. Eliceiri, Dual-stream multiple instance learning network for whole slide image classification with self-supervised contrastive learning, in: *Proceedings of the IEEE/CVF conference on computer vision and pattern recognition*, 2021, pp. 14318–14328.
- [12] M. Y. Lu, D. F. Williamson, T. Y. Chen, R. J. Chen, M. Barbieri, F. Mahmood, Data-efficient and weakly supervised computational pathology on whole-slide images, *Nature biomedical engineering* 5 (2021) 555–570.
- [13] Z. Su, T. E. Tavalara, G. Carreno-Galeano, S. J. Lee, M. N. Gurcan, M. Niazi, Attention2majority: Weak multiple instance learning for regenerative kidney grading on whole slide images, *Medical Image Analysis* 79 (2022) 102462.
- [14] L. Qu, X. Luo, S. Liu, M. Wang, Z. Song, Dgmil: Distribution guided multiple instance learning for whole slide image classification, in: *International Conference on Medical Image Computing and Computer-Assisted Intervention*, Springer, 2022, pp. 24–34.
- [15] P. Chikontwe, S. J. Nam, H. Go, M. Kim, H. J. Sung, S. H. Park, Feature re-calibration based multiple instance learning for whole slide image classification, in: *International Conference on Medical Image Computing and Computer-Assisted Intervention*, Springer, 2022, pp. 420–430.
- [16] T. E. Tavalara, M. N. Gurcan, M. K. K. Niazi, Contrastive multiple instance learning: An unsupervised framework for learning slide-level representations of whole slide histopathology images without labels, *Cancers* 14 (2022) 5778.
- [17] T. Chen, S. Kornblith, M. Norouzi, G. Hinton, A simple framework for contrastive learning of visual representations, in: *International conference on machine learning*, PMLR, 2020, pp. 1597–1607.
- [18] J. Zbontar, L. Jing, I. Misra, Y. LeCun, S. Deny, Barlow twins: Self-supervised learning via redundancy reduction, in: *International Conference on Machine Learning*, PMLR, 2021, pp. 12310–12320.
- [19] H. Zhang, M. Cisse, Y. N. Dauphin, D. Lopez-Paz, mixup: Beyond empirical risk minimization, *arXiv preprint arXiv:1710.09412* (2017).
- [20] V. Verma, A. Lamb, C. Beckham, A. Najafi, I. Mitliagkas, D. Lopez-Paz, Y. Bengio, Manifold mixup: Better representations by interpolating hidden states, in: *International conference on machine learning*, PMLR, 2019, pp. 6438–6447.
- [21] R. J. Chen, C. Chen, Y. Li, T. Y. Chen, A. D. Trister, R. G. Krishnan, F. Mahmood, Scaling vision transformers to gigapixel images via hierarchical self-supervised learning, in: *Proceedings of the IEEE/CVF Conference on Computer Vision and Pattern Recognition*, 2022, pp. 16144–16155.
- [22] C. Zhang, Y. Gu, Dive into self-supervised learning for medical image analysis: Data, models and tasks, *arXiv preprint arXiv:2209.12157* (2022).
- [23] O. Ciga, T. Xu, A. L. Martel, Self supervised contrastive learning for digital histopathology, *Machine Learning with Applications* 7 (2022) 100198.
- [24] R. J. Chen, R. G. Krishnan, Self-supervised vision transformers learn visual concepts in histopathology, *arXiv preprint arXiv:2203.00585* (2022).
- [25] K. He, X. Zhang, S. Ren, J. Sun, Deep residual learning for image recognition, in: *Proceedings of the IEEE conference on computer vision and pattern recognition*, 2016, pp. 770–778.
- [26] A. Dosovitskiy, L. Beyer, A. Kolesnikov, D. Weissenborn, X. Zhai, T. Unterthiner, M. Dehghani, M. Minderer, G. Heigold, S. Gelly, et al., An image is worth 16x16 words: Transformers for image recognition at scale, *arXiv preprint arXiv:2010.11929* (2020).
- [27] M. Caron, H. Touvron, I. Misra, H. Jégou, J. Mairal, P. Bojanowski, A. Joulin, Emerging properties in self-supervised vision transformers, in: *Proceedings of the IEEE/CVF international conference on computer vision*, 2021, pp. 9650–9660.
- [28] M. Kang, H. Song, S. Park, D. Yoo, S. Pereira, Benchmarking self-supervised learning on diverse pathology datasets, in: *Proceedings of the IEEE/CVF Conference on Computer Vision and Pattern Recognition*, 2023, pp. 3344–3354.
- [29] M. Caron, I. Misra, J. Mairal, P. Goyal, P. Bojanowski, A. Joulin, Unsupervised learning of visual features by contrasting cluster assignments, *Advances in neural information processing systems* 33 (2020)

- 9912–9924.
- [30] X. Chen, H. Fan, R. Girshick, K. He, Improved baselines with momentum contrastive learning, *arXiv preprint arXiv:2003.04297* (2020).
- [31] B. Wong, M. Y. Yi, Rethinking pre-trained feature extractor selection in multiple instance learning for whole slide image classification, *arXiv preprint arXiv:2408.01167* (2024).
- [32] J. Yang, H. Chen, Y. Zhao, F. Yang, Y. Zhang, L. He, J. Yao, Remix: A general and efficient framework for multiple instance learning based whole slide image classification, in: *International Conference on Medical Image Computing and Computer-Assisted Intervention*, Springer, 2022, pp. 35–45.
- [33] Z. Shao, H. Bian, Y. Chen, Y. Wang, J. Zhang, X. Ji, et al., Transmil: Transformer based correlated multiple instance learning for whole slide image classification, *Advances in neural information processing systems* 34 (2021) 2136–2147.
- [34] H. Zhang, Y. Meng, Y. Zhao, Y. Qiao, X. Yang, S. E. Coupland, Y. Zheng, Dtd-mil: Double-tier feature distillation multiple instance learning for histopathology whole slide image classification, in: *Proceedings of the IEEE/CVF Conference on Computer Vision and Pattern Recognition*, 2022, pp. 18802–18812.
- [35] W. Tang, S. Huang, X. Zhang, F. Zhou, Y. Zhang, B. Liu, Multiple instance learning framework with masked hard instance mining for whole slide image classification, in: *Proceedings of the IEEE/CVF International Conference on Computer Vision*, 2023, pp. 4078–4087.
- [36] N. Hashimoto, D. Fukushima, R. Koga, Y. Takagi, K. Ko, K. Kohno, M. Nakaguro, S. Nakamura, H. Hontani, I. Takeuchi, Multi-scale domain-adversarial multiple-instance cnn for cancer subtype classification with unannotated histopathological images, in: *Proceedings of the IEEE/CVF conference on computer vision and pattern recognition*, 2020, pp. 3852–3861.
- [37] W. Hou, L. Yu, C. Lin, H. Huang, R. Yu, J. Qin, L. Wang, H²-mil: exploring hierarchical representation with heterogeneous multiple instance learning for whole slide image analysis, in: *Proceedings of the AAAI conference on artificial intelligence*, volume 36, 2022, pp. 933–941.
- [38] G. Bontempo, F. Bolelli, A. Porrello, S. Calderara, E. Ficarra, A graph-based multi-scale approach with knowledge distillation for wsi classification, *IEEE Transactions on Medical Imaging* (2023).
- [39] C. Shorten, T. M. Khoshgoftaar, A survey on image data augmentation for deep learning, *Journal of big data* 6 (2019) 1–48.
- [40] A. Galdran, G. Carneiro, M. A. González Ballester, Balanced-mixup for highly imbalanced medical image classification, in: *Medical Image Computing and Computer Assisted Intervention–MICCAI 2021: 24th International Conference, Strasbourg, France, September 27–October 1, 2021, Proceedings, Part V 24*, Springer, 2021, pp. 323–333.
- [41] J.-R. Chang, M.-S. Wu, W.-H. Yu, C.-C. Chen, C.-K. Yang, Y.-Y. Lin, C.-Y. Yeh, Stain mix-up: Unsupervised domain generalization for histopathology images, in: *Medical Image Computing and Computer Assisted Intervention–MICCAI 2021: 24th International Conference, Strasbourg, France, September 27–October 1, 2021, Proceedings, Part III 24*, Springer, 2021, pp. 117–126.
- [42] S. Ren, H. Wang, Z. Gao, S. He, A. Yuille, Y. Zhou, C. Xie, A simple data mixing prior for improving self-supervised learning, in: *Proceedings of the IEEE/CVF conference on computer vision and pattern recognition*, 2022, pp. 14595–14604.
- [43] Y.-C. Chen, C.-S. Lu, Rankmix: Data augmentation for weakly supervised learning of classifying whole slide images with diverse sizes and imbalanced categories, in: *Proceedings of the IEEE/CVF Conference on Computer Vision and Pattern Recognition*, 2023, pp. 23936–23945.
- [44] P. Liu, L. Ji, X. Zhang, F. Ye, Pseudo-bag mixup augmentation for multiple instance learning-based whole slide image classification, *IEEE Transactions on Medical Imaging* (2024).
- [45] K. Weiss, T. M. Khoshgoftaar, D. Wang, A survey of transfer learning, *Journal of Big data* 3 (2016) 1–40.
- [46] A. Paszke, S. Gross, F. Massa, A. Lerer, J. Bradbury, G. Chanan, T. Killeen, Z. Lin, N. Gimelshein, L. Antiga, et al., Pytorch: An imperative style, high-performance deep learning library, *Advances in neural information processing systems* 32 (2019).
- [47] B. E. Bejnordi, M. Veta, P. J. Van Diest, B. Van Ginneken, N. Karssemeijer, G. Litjens, J. A. Van Der Laak, M. Hermsen, Q. F. Manson, M. Balkenhol, et al., Diagnostic assessment of deep learning algorithms for detection of lymph node metastases in women with breast cancer, *Jama* 318 (2017) 2199–2210.
- [48] M. J. Ellis, M. Gillette, S. A. Carr, A. G. Paulovich, R. D. Smith, K. K. Rodland, R. R. Townsend, C. Kinsinger, M. Mesri, H. Rodriguez, et al., Connecting genomic alterations to cancer biology with proteomics: the nci clinical proteomic tumor analysis consortium, *Cancer discovery* 3 (2013) 1108–1112.
- [49] D. Wang, Y. Shang, A new active labeling method for deep learning, in: *2014 International joint conference on neural networks (IJCNN)*, IEEE, 2014, pp. 112–119.
- [50] D. Arthur, S. Vassilvitskii, K-means++ the advantages of careful seeding, in: *Proceedings of the eighteenth annual ACM-SIAM symposium on Discrete algorithms*, 2007, pp. 1027–1035.
- [51] O. Sener, S. Savarese, Active learning for convolutional neural networks: A core-set approach, *arXiv preprint arXiv:1708.00489* (2017).
- [52] J. T. Ash, C. Zhang, A. Krishnamurthy, J. Langford, A. Agarwal, Deep batch active learning by diverse, uncertain gradient lower bounds, *arXiv preprint arXiv:1906.03671* (2019).
- [53] S. Agarwal, H. Arora, S. Anand, C. Arora, Contextual diversity for active learning, in: *Computer Vision–ECCV 2020: 16th European Conference, Glasgow, UK, August 23–28, 2020, Proceedings, Part XVI 16*, Springer, 2020, pp. 137–153.
- [54] A. Goode, B. Gilbert, J. Harkes, D. Jukic, M. Satyanarayanan, Openslide: A vendor-neutral software foundation for digital pathology, *Journal of pathology informatics* 4 (2013) 27.
- [55] C. Grisi, Histopathology slide pre-processing pipeline, <https://github.com/clemmgrs/hs2p>, 2023. [Accessed 10-10-2023].
- [56] Y. You, I. Gitman, B. Ginsburg, Large batch training of convolutional networks, *arXiv preprint arXiv:1708.03888* (2017).
- [57] D. P. Kingma, J. Ba, Adam: A method for stochastic optimization, *arXiv preprint arXiv:1412.6980* (2014).